

Aspheric glass lens modeling and machining

R. Barry Johnson^a, SPIE Fellow and Life Member, and Michael Mandina^b, SPIE Member

^aCyberAir Development Corporation, 3077-K Leeman Ferry Rd., Huntsville, AL 35801, USA

^bOptimax Systems, Inc., 6367 Dean Parkway, Ontario, NY 14519, USA

ABSTRACT

The incorporation of aspheric lenses in complex lens system can provide significant image quality improvement, reduction of the number of lens elements, smaller size, and lower weight. Recently, it has become practical to manufacture aspheric glass lenses using diamond-grinding methods. The evolution of the manufacturing technology is discussed for a specific aspheric glass lens. When a prototype all-glass lens system (80 mm efl, F/2.5) was fabricated and tested, it was observed that the image quality was significantly less than was predicted by the optical design software. The cause of the degradation was identified as the large aspheric element in the lens. Identification was possible by precision mapping of the spatial coordinates of the lens surface and then transforming this data into an appropriate optical surface defined by derived grid sag data. The resulting optical analysis yielded a modeled image consistent with that observed when testing the prototype lens system in the laboratory. This insight into a localized slope-error problem allowed improvements in the fabrication process to be implemented. The second fabrication attempt, the resulting aspheric lens provided remarkable improvement in the observed image quality, although still falling somewhat short of the desired image quality goal. In parallel with the fabrication enhancement effort, optical modeling of the surface was undertaken to determine how much surface error and error types were allowable to achieve the desired image quality goal. With this knowledge, final improvements were made to the fabrication process. The third prototype lens achieved the goal of optical performance. Rapid development of the aspheric glass lens was made possible by the interactive relationship between the optical designer, diamond-grinding personnel, and the metrology personnel. With rare exceptions, the subsequent production lenses were optical acceptable and afforded reasonable manufacturing costs.

Keywords: Aspheric, lens, optical manufacturing, lens design, metrology, fabrication, diamond grinding

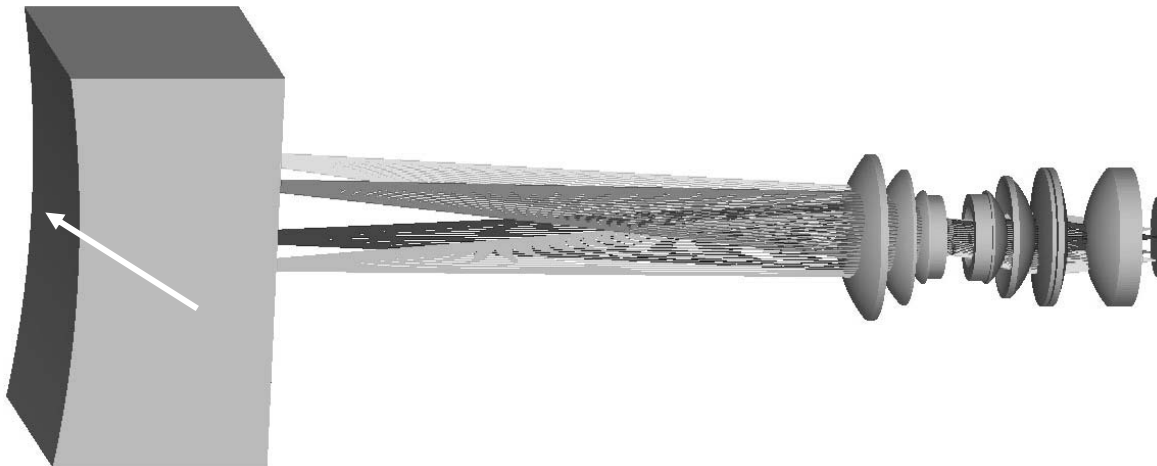


Figure 1. Optical configuration.

1. INTRODUCTION

The transition from film to electronic media in recent years rapidly increased the demanding performance requirements of telecine transfer machines. Such machines scan the film to create electronic signals having high fidelity. There are several viable approaches to accomplishing the telecine function; however, only the so-called flying spot approach was considered in this investigation. This system comprises a very high-quality CRT, an imaging lens (often called a Gate Lens), film gate, detectors, processing electronics, and the recording medium (video tape, digital data storage, etc.). The system basically functions in the following manner. The film gate positions a frame of film such that a very small, but intense, spot of quasi-white light generated by the CRT can be scanned in a line-by-line manner over the frame of film. The CRT spot light source is imaged by a high-quality lens to demagnify the spot size. The light passing through the film frame is then captured by a light sensor assembly, which converts the several spectral bands into appropriate electrical signals for recording. The electronics for control and signal processing are quite complex and advanced. Each part of the telecine system has exacting and challenging specifications.

Figure 1 shows the layout of the new Gate Lens for 35-mm film format, with double frame height, which can accommodate VISTA VISION (8 perf 35 mm), and was designed and fabricated for certain upgraded and new technology telecine machines. The developed lens is a telecentric, 10-element apochromat lens having a focal length of 80 mm, operating at a magnification of -0.25 , $F/2.5$, and optimized for the specific faceplate and film-gate skid-plate curvatures. The spectral response of the lens is significantly broader than conventional telecine lenses to better match the film and new CRT spectrums. For certain system reasons, the interior surface of the CRT faceplate (see arrow in Fig. 1) and the film skid plate were made cylindrical, which made the design challenge ever more interesting.¹

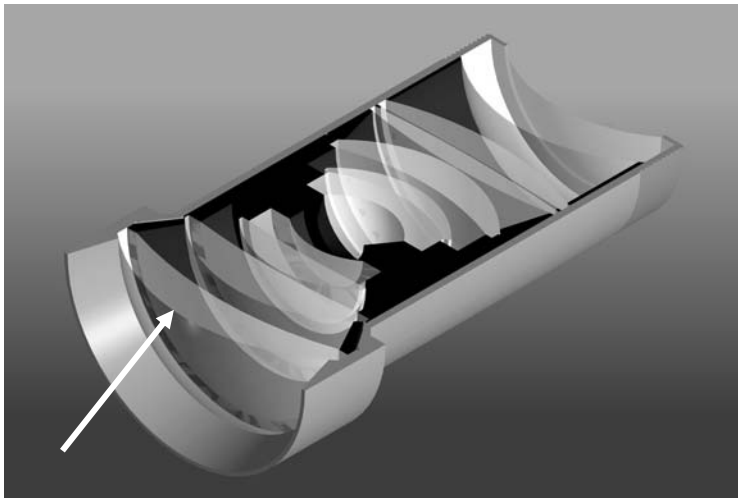


Figure 2. Cut-away view of the lens assembly.



Figure 3. Exploded view of lens system assembly.

The lens assembly had to mechanically fit in a rather confined space with respect to the CRT and film gate. The lens is held within the film gate body and utilized all available diameter and length. In order to achieve the desired mechanical and optical performance objectives, it was quickly determined that at least one aspheric lens surface would be required. The incorporation of aspheric lenses in complex lens system can provide significant image quality improvement, reduction of the number of lens elements, smaller size, and lower weight. As can be observed in the rendering cut-away view of the lens assembly shown in Fig. 2, the lens assembly is densely packed with lens elements. The mechanical design of the lens barrel, lens holders, and spacers was highly integrated to reduce size, weight, cost, and alignment

¹ The skid plate in the film gate is a convex cylinder to the right as viewed in Fig. 1 so that the film can be moved quickly and safely during the transfer process. It is readily seen that a cylindrical surface (same radius scaled by the ratio of the refractive indices) must be located on the interior surface of the CRT (location of the phosphors) by invoking the Lagrange invariant.^[1] It is interesting to note that the radius is not determined by the lens magnification; however, since the index of refraction is different in object and image space, then the radii are related by the ratio of these refractive indices. The surface on the CRT is of course concave.

difficulties. Figure 3 is a rendering of an exploded view of the lens system assembly. After evaluating the basic design of the optics, it was determined that only a single 10th-order aspheric surface was needed and the most effective location was on the first surface of the first lens element (see arrow in Fig. 2).

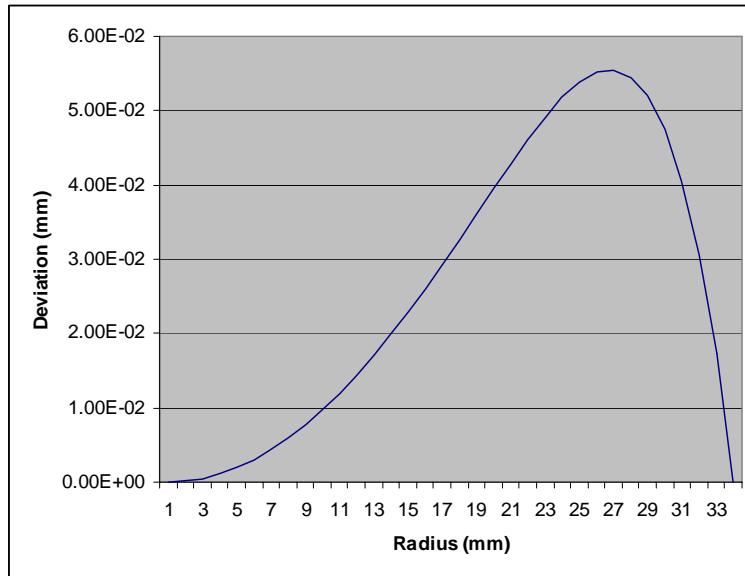


Figure 4. Deviation of aspheric surface from best-fit spherical surface.

This paper discusses the evolution of the manufacturing technology for the aspheric glass lens rather than the lens design. Around the year 2000, the manufacture of relatively aspheric glass lenses was typically a costly and time consuming process. Since the Gate Lens needed to be rapidly developed and then transitioned into production at an acceptable cost, Johnson investigated with Optimax Systems, Inc., before the actual design, the practicality of volume production such a lens using diamond-grinding technology, which was a relatively new technology at the time. The basic guidelines determined for the design of the aspheric lens were that only certain glass types should be used, the surface should be convex, the element diameter should not be too small, the element should be thick enough to allow the surface to remain stable during manufacture and use, and the aspheric deviation from the base surface should be smooth and not contain any “concave” deviations. Figure 4 presents the deviation of aspheric surface from best-fit spherical surface, and it is evident that the deviation guidelines were met. Note that the maximum deviation is about 55 μm . The other guidelines were also met.

2. DESIGN

The design of the Gate Lens primarily utilized the ZEMAX Optical Design Program. After a basic Double-Gauss configuration was determined that yielded reasonably acceptable optical performance and met the mechanical restrictions, the final push to achieve the desired optical performance was made by attempting to locate where an aspheric surface could be acceptably placed for manufacture by diamond grinding. As mention previously, the convex surface of the first element was identified. It was determined, in consultation with Optimax, that SF15 was a viable glass for diamond grinding and worked acceptably in the optical design (although not the optimum glass). The aspheric lens element has a clear aperture of about 66 mm and center thickness of 10 mm.

Two questions that both the lens design and lens fabricator must address are the surface figure tolerance and the surface finish. Although the ZEMAX tolerance analysis provides reasonably good insight into lens systems containing spherical-only surfaces, it was difficult to specify the tolerance for the aspheric surface. The tolerance was estimated by deforming the surface profile by controlled amounts so that ultimately a peak-to-valley tolerance was set with an understanding that the slope error had to vary in a smooth manner without extreme spatial changes.

3. GLASS ASPHERIC LENSES GRINDING AND POLISHING TECHNOLOGY

3.1. Manufacturability Considerations

Quality levels for precision aspheres continue to improve each year. Optics manufacturers have a growing selection of asphere processing machine tools available. Most of these modern asphere manufacturing systems can produce surface figures within 3 fringes of irregularity routinely; however, fractional wave requirements often require a combination of expert optician skill and secondary operations on state of the art (and possibly proprietary) equipment. The issue of localized slope error in the form of undulations described prior is a potential process artifact that the designer should consider when designing an aspheric surface into a lens system. The following subsections provide an overview of some lens parameters for designers who are contemplating designing with aspheres.

3.2. Diameter (Size)

Designers generally have a growing number of aspheric lens suppliers producing lenses in the 10 mm to 100 mm diameter range. As diameter increases, the number of suppliers decreases dramatically. The decreasing number is primarily driven by two factors. First, the grinding equipment required for larger diameter aspheres is extremely rigid and precise. Larger parts require larger machine tools that can properly dampen the resulting larger dynamic forces from spindles and drive systems. Second, flexible metrology systems such as the Taylor Hobson Talysurf, are limited to 120 mm or 200 mm scan lengths depending on model. When the aperture requirements exceed vendor metrology capability, aspheres cannot be reliably produced.

3.3. Material

Most materials that are processed into spherical shapes can be made into aspheres; however, because of the higher manufacturing costs associated with aspheres, it is strongly recommended designers use robust materials whenever possible. For example, materials that are more sensitive chemically and stain easily will be more problematic. Materials prone to fracture from bonded diamond tool grinding such as any glass type that ends with 50 or higher should be avoided, for example FK51, S-FPL51, 52, and 53. It is best to select materials that yield minimal subsurface damage after the grinding operation. This will enhance the opportunity for the shortest possible polishing time. Longer run times in the polishing phase are costly and may aggravate asymmetries and cause harmonic undulations similar to scan to be presented in Fig 10. Some preferred materials are Fused Silica, BK7, SFL6, SSKN5, SK4, and SF15. For the Gate Lens aspheric, SF15 was used.

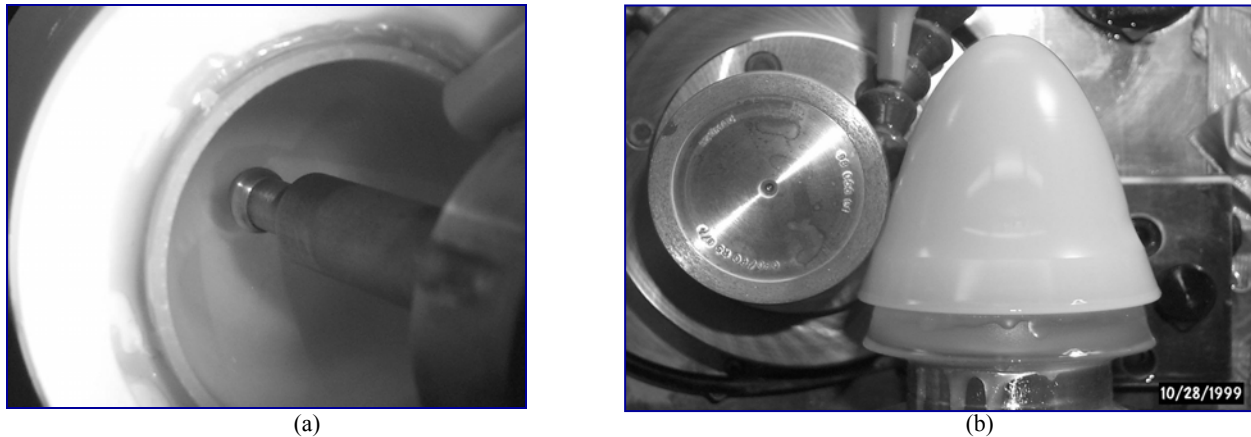


Figure 5. Complex part processed at the Center for Optics Manufacturing, Rochester, NY.

3.4. Asphere Geometry: Concave vs. Convex Aspheric Surfaces

Simply stated, a convex aspheric surface is easier to manufacture than a concave surface. An aspheric surface that cannot be shaped by a grinding wheel of infinite radius (i.e., a plane) will have increased manufacturing cost. This precludes any non-convex asphere or any convex asphere containing a point of inflection. In most cases, aspheric surfaces are ground using diamond ring tools or peripheral grinding wheels. The grinding occurs essentially at a point

tangent to both the grinding tool's cutting surface and the convex asphere lens. In a short time, the grinding wheel wears and the contact point becomes a zone. The actual grinding dimensional parameters change as the tool is consumed in the process. A larger the tool diameter involves more diamond-cutting points per revolution enabling a more robust grinding process. Consequently, the lesser wear allows the tool to hold the its original dimensions and shape longer. Tools 100 mm in diameter are common.

Any concave shape on an aspheric form will limit the peripheral grinding wheel diameter. This could be an inflected region on a seemingly convex part. It is possible to use smaller diameter tools, but if your design requires a tool radius less than 20 mm, you are limiting the number of process methods available to produce your part. Most modern asphere polishing machines have concave radius limits. For example, the A-II asphere polisher from LOH and Schneider's polisher have a 20 mm concave lens radius limit, while QED's magnetorheological finishing (MRF) limit is 13mm. Figure 5 shows two extreme examples of parts processed at COM (Center for Optics Manufacturing). Note the relatively small spherical radius of the tool used to grind a deep parabolic shape in the first image. The concave asphere shown in Fig. 5(a) is more complex and costly to manufacture than the corresponding convex shape shown in Fig. 5(b).

3.5. Form / Slope (F/#)

There are a number of considerations that will help the designer and the fabricator optimize overall system cost and performance. When selecting the form equation, it is always better to use even powers than odd powers. Defining the aspheric shape using R ($1/c$), K (conic constant), and A4 through A10 (aspheric terms through 10th order) are the most manageable. Higher order aspheric terms (A12 thru A20) can cause the aspheric shape to become more complex and expensive to produce, and in some cases, non-manufacturable due to asymptotic influence and or inflections. These terms change the shape essentially near the periphery of the part. The fewer terms used and the fewer numbers required, the less likely a data entry error will be made in the various stages of fabrication and test. By providing a sag table, the fabricator is helped to ensure that the lens prescription will not be misinterpreted and can be verified numerically prior to manufacture or measurement. Fabricators typically type the aspheric form values into various keyboard front-ends. For example, spread sheet software, one or two deterministic grinders, one or two CNC polishers, and one or two metrology devices. Each of these 4 to 7 interface data entry points is an opportunity for error.

Once the form has been established, it is useful to check that it is well behaved 4 mm beyond the clear aperture. Most grinding wheels and polishing pads require a smooth transition off the part. The aspheric surface may be well behaved within the clear aperture, but the designer should check the surface behavior 3 to 5 mm beyond the clear aperture. If it inflects and goes asymptotic, that usually presents a manufacturing problem. It could also complicate the mount design. As the F/# becomes faster, mating the multi-stage grind operations become much more challenging. Thickness control is more difficult and there may be annular zones of poor polish as uniform removal is made more difficult by the radical shape. Slopes that exceed 45 degrees from the plane perpendicular to the axis add other difficulties. For example: the profilometer probe has a tendency to flex as the slope increases, especially on the downward slope, which can yield false asymmetry measurements. Additionally, the ability to use interferometers to measure surfaces, especially convex surfaces is further hampered with increased slope.

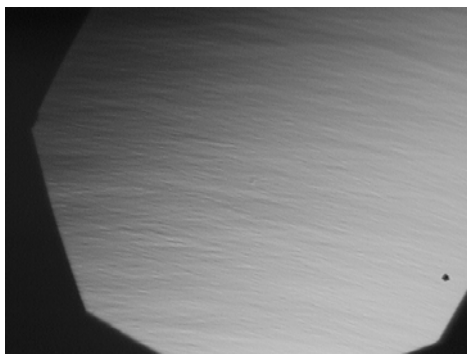


Figure 6.

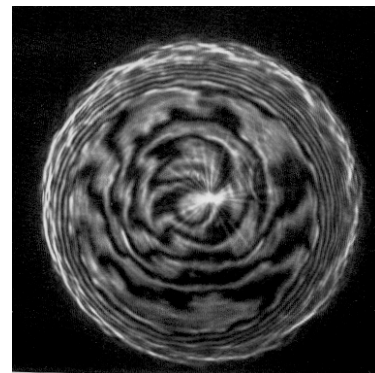


Figure 7

3.6. Surface Figure and Finish

Final finishing of the ground aspheric surface is accomplished using standard rouges and materials. The primary difference is the lap. Where spherical surfaces are polished with essentially full contact laps, aspheres are polished in small zones using flexible laps. Most surfaces presented to the polishing operation are imperfect. The ground surfaces may have residual artifacts on the surface that are by-products of the grinding operation. It is not uncommon to observe mild waves and pockets on the surface.

Figure 6 is an image of a polished aspheric surface taken with a Nomarski Microscope at 50X midway through the polishing process. Note the surface texture and mid-spatial sinusoidal-like undulations radiating out from the bottom of the image to the top. Figure 7 is an interferogram of the aspheric form shown in Fig.6. Note the asymmetry and the mottled look caused by the fractional wave localized slope errors. Bearing noise, vibration, motion control and other process characteristics from the grinding operation all contribute to inducing these localized mid-spatial-frequency form errors. The polishing process removes the grinding damage, and corrects form irregularities. It is important to polish using a flexible pad that will essentially wear down the undulation peaks. Pads that are too soft or compliant will follow the contour left by the grind wheel and fail to reduce the mid-spatial-frequency defects. Polishing too long may leave a signature pattern on the surface that must be mitigated using alternative pads and smoothing methods. Ultimately, the surface uniformity and slope error are rarely as good as a comparable spherical lens surface; a point of importance.

For designs that require fractional wave surfaces, there is an advantage to designing aspheric forms that are within $5\ \mu\text{m}$ departure of a best-fit-sphere. Depending on equipment and process sophistication, it is often possible to correct a polished spherical surface to a well-corrected aspheric shape in less time and with higher precision when the aspheric form is close to spherical. Usually a phase-measuring interferometer equipped with a standard transmission sphere is adequate to obtain surface profile information that can be provided to the deterministic polisher.

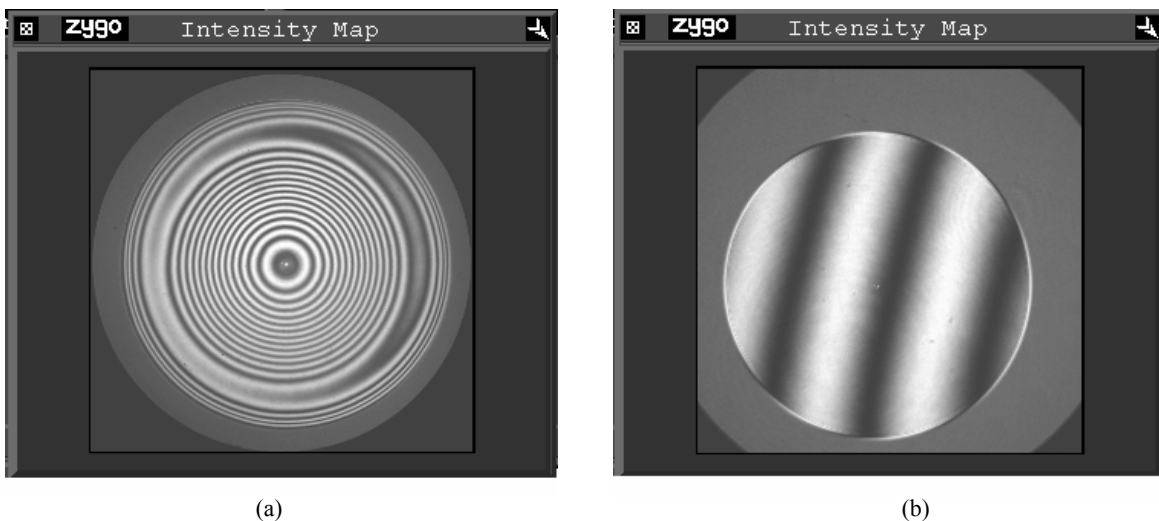


Figure 8. (a) is an interferogram of a 68-mm diameter aspheric surface in reflection using a 4" F/3.2 transmission sphere and (b) is the interferogram of the resulting double pass transmitted wavefront error.

The Taylor Hobson Form TalySurf has been the metrology device of choice for asphere manufactures for the last decade. This was the device used during the development of the aspheric lens for the Gate Lens. The TalySurf measures a two-dimensional profile by "dragging" a cantilevered stylus across the surface of the asphere. It measures position of the stylus as it moves across the surface and through the vertex of the asphere. The software "best fits" the theoretical form to the actual, accommodating for squareness errors between the aspheric axis and the direction of stylus motion. The TalySurf is able to generate any theoretical aspheric form containing terms up to twentieth order. Its limits are more physical in nature. Presently any surface containing more than 25 mm in sag over the aperture of interest can not be measured. Additionally, form accuracy is traded for sag range. A stylus that permits more sag to be measured has more uncertainty in the measurement than one that permits less sag to be measured.

It is critical that the scan exceeds clear aperture requirements, since the resulting surface data file is used to calculate machine parameters in both the grinding and polishing operations. Tool path must be defined for several millimeters beyond the usable aperture and so must form error. Rotational asymmetries can be identified and characterized by taking intersecting scans of the same surface; however, few manufactures are capable of using this information for deterministic correction of asymmetries. Most must maintain rotational symmetry at all cost and correct form error based on a single scan.

3.7. Alignment and Centration

Optics fabrication technicians who are not familiar with aspheric lenses often fail to realize that the aspheric surface has its own axis. The edging operation where the diameter is ground to final dimension must have a means for locating the aspheric axis on the edging machine's rotational axis. Traditional methods that rely on indicators or optical systems are often not sufficient because a tilted asphere at times can appear to be well aligned by both methods. Assuming a spherical radius on the other side, that center of radius must be located on the aspheric axis prior to the final edging operation. Unlike a spherical lens where the edging operation establishes the alignment of the element by locating the center of radii on the edging machines rotational axis, the aspheric-spheric lens must be already aligned. The edging operation simply brings the diameter to final dimension.

Sag	< 10 mm	10-20 mm	> 20 mm*
Form Error			
Commercial	± 5 µm	± 5 µm	± 10 µm
Precision	± 1 µm	± 1 µm	± 2 µm
Mfg Limits	± 0.5 µm	± 1 µm	± 1 µm
Slope Error			
Commercial	> 2 µm / mm	> 2 µm / mm	> 3 µm / mm
Precision	1 µm / mm	1 µm / mm	2 µm / mm
Mfg Limits	0.3 µm / mm	0.6 µm / mm	1 µm / mm
Max. Head Angle	60°	60°	60°

* Talysurf maximum sag range = 25 mm

Table 1. Aspheric surface tolerances.

3.8. Optimax Asphere Tolerance Matrix

Table 1 provides fabrication guidance to asphere designers where contact profilometry is utilized. This table is based upon years of experience and lessons learned.

4. FABRICATION AND EVALUATION

Before committing the design to production, a single prototype lens was fabricated to validate the Gate Lens performance. Optimax specializes in rapid prototyping of high-quality lenses. The first set of lenses was produced in less than a month after the design was released. Of course, the selection of the various glasses were frozen prior to the competition of the design so that they could be ordered and be on hand when fabrication began. The most difficult of the lens elements to fabricate was the aspheric element. At the same time the lenses were being made, the mechanical components design was completed and the parts were fabricated at a local machine shop in Huntsville, Alabama. These parts for the prototype were produced without difficulty.

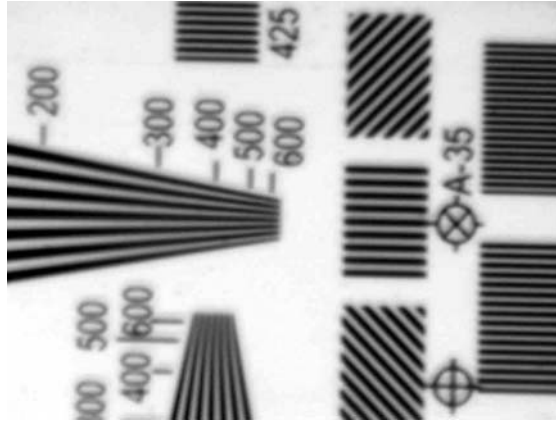


Figure 9. Image of the standard test formed by the first prototype Gate Lens.

Once the mechanical parts and the lenses were received, the prototype Gate Lens was assembled without difficulty. Due to the very-high value of a telecine transfer machine, it was decided that not to use one for initial evaluation of the lens. Instead, a test set was constructed that comprised the faceplate from an actual system CRT, the Gate Lens under test, an actual film gate to hold the lens and provide the focus mechanism, standard TV-resolution test film strip, a diffuse illuminating source of the film. The prototype lens forms an image of the resolution target on the CRT faceplate phosphor surface. The faceplate is very thick to mitigate effects of dust. Testing requires the faceplate be included since the lens design included this component and it does impact the overall performance of the lens system. The image formed on the faceplate was viewed by a color TV camera having a 4X microscope objective, a frame grabber, and a display. Frames were stored on the computer for later analysis. When the image formed by the first prototype lens was viewed, see Fig. 9, it was apparent that the performance fell far short of that expected. The image obtained was very “soft” and indicated something was in error.

To identify the source of the problem, the lens was disassembled and all of the mechanical parts were again carefully measured to be sure that they were within tolerance. In fact, the parts were very close to their nominal values. Next, the lenses were checked by examination of the QA report for each spherical lens element. Again, they were all within tolerance and close to the nominal values. This left the aspheric surface as the most likely cause. Now the questions were how to first verify that this was indeed the problem and second how to resolve the matter.

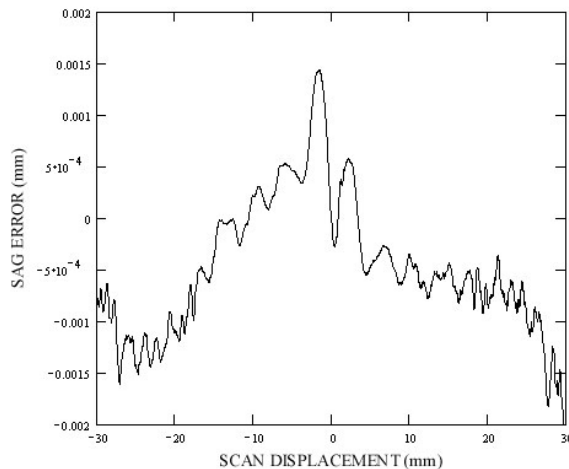


Figure 10. Radial mechanical profilometer scan across the diameter of the aspheric lens surface with respect to the design surface shape. Note the undulations.

The first step was to examine the aspheric surface carefully. Optimax made a profilometer scan across the diameter of the aspheric lens surface with the resulting data shown in Fig. 10. Three observations can be made from examination of this data. First, the peak-to-valley error is greater than desired. Second, there are rather rapid undulations of just under $0.5 \mu\text{m}$. And third, the scan is asymmetric. A visual inspection of the lens surface under appropriate lighting revealed an observable pattern consistent with the radial scan data.

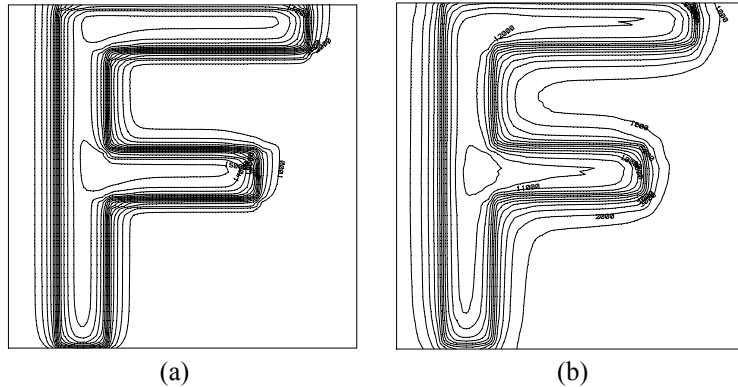


Figure 11. Contour plots of the modeled image of the letter “F” where (a) is the plots for the lens having the design parameters and (b) is the plot for the first prototype lens. The length of each side of the enclosing box is 0.13 mm.

The next step was to attempt to model the lens surface to determine if the modeled Gate Lens performance, having the aforementioned surface errors, was generally consistent with the observed test target image. The objective was to use the model to gain a greater insight into the surface-error problem so that improvements in the fabrication process could be implemented. ZEMAX includes a surface description denoted as grid sag. This surface shape is defined by a base plane, sphere, conic asphere, and/or polynomial asphere plus additional sag terms defined by a rectangular array of sag values. The resultant surface shape is determined by a bicubic spline interpolation of the sag values. More details can be found in the ZEMAX User’s Manual.

Since the profilometer scan showed an asymmetric nature to the surface, the generation of the two-dimensional sag data is more complex than had the surface error been symmetric. The cause of the asymmetry was due to the initial fabrication process. Although not rigorously valid, the scan shown in Fig. 10 was assumed to be the worse-case deformation errors. In order to transform the asymmetric radial surface deformation data into rectilinear data needed for grid sag surface input, a Mathcad program was written and is provided in the Appendix. Figure 11 shows contour plots of the letter “F” (0.133 mm image height) for the design lens and first prototype lens. As can be seen, the expected design image (Fig. 11 (a)) is quite good while the modeled image of the prototype lens (Fig. 11 (b)) is rather soft. This is consistent with the actual image, formed by the prototype lens, of the test target shown in Fig. 9.

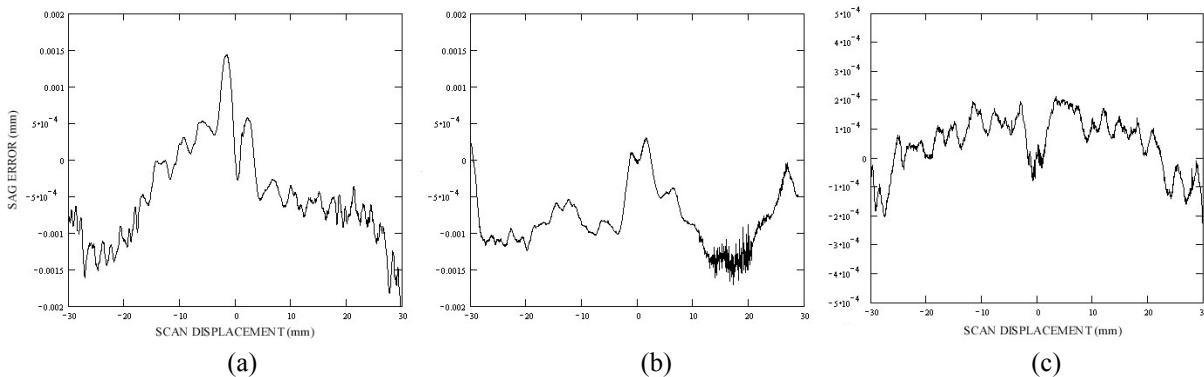


Figure 12. Surface displacement error scans referenced to desired surface form. The original lens is (a), the repolished lens is (b), and the remade lens is (c). Note that sag error scale is different for (c) that (a) or (b).

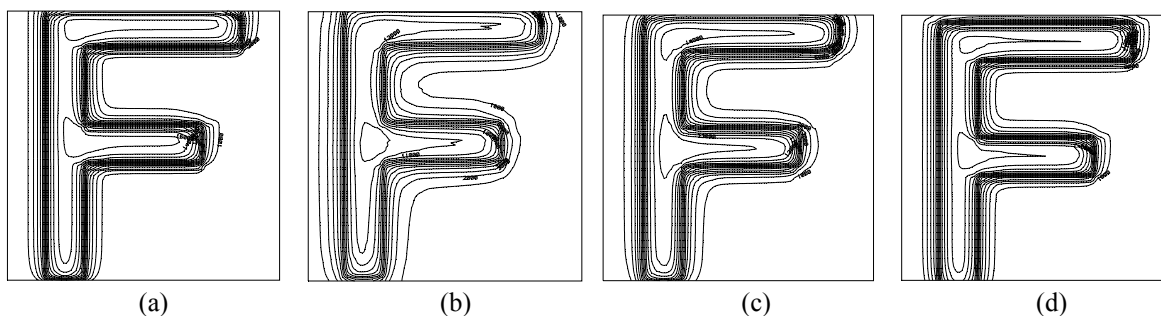


Figure 13. Diffraction image analysis of lens is shown for (a) the design performance, (b) with the original aspheric lens, (c) with the repolished aspheric lens, and (d) with the remade aspheric lens. The size of the box containing the letter “F” is 0.133 mm by 0.133 mm.

Now that a model was available that was generally consistent with laboratory observations, it was used to better understand how good the surface figure had to be to achieve the desired performance. The model indicated that much of the image softness was due to the undulations evident in Fig. 10. By reducing these undulations significantly, the model indicated a much improved image should be obtained. The first approach tried was to repolish the surface of the prototype lens in an attempt to remove the undulations to the extent practicable. Figure 12(b) shows that the undulations have been reduced in both frequency and amplitude. Figure 13(c) illustrates a definite improvement of the modeled image when compared to the original prototype modeled image (Fig. 13(b)) and is nearing the desired image shown in Fig. 13(a). At this point, it was decided that no additional improvement of the original prototype lens surface could be obtained, so a second prototype, or remade, lens was fabricated utilizing the evolving and improving fabrication techniques. A profilometer scan of the repolished lens is shown in Fig. 12(c). Notice the very great improvement in surface figure and quality. The undulations are still present, but they and the surface figure error are within acceptable values. Examination of the contour plot of the letter “F”, shown in Fig. 13(d), when the remade lens is used illustrates an image essentially equivalent to the desired design image.

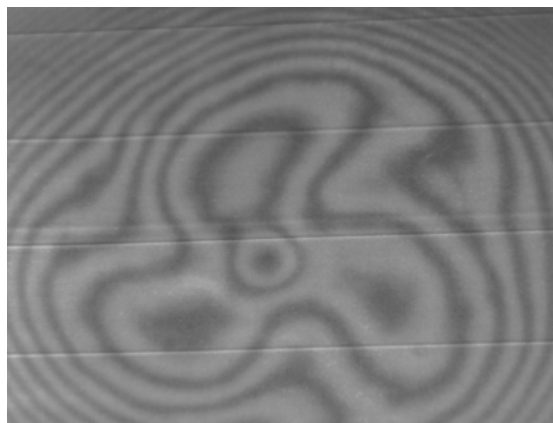


Figure 14.

At the time Optimax initiated the manufacturing of the Gate Lens system, its grinding capability consisted of older CNC Opticam platforms. Motion control was accurate to a $1\ \mu\text{m}$, so form error across the surface was ultimately within several microns. Unfortunately radially propagated sinusoidal undulations remained after the final grinding operation, and it was these undulations that ultimately degraded overall system performance. The polishing process tended to lower the undulations amplitude, but did not remove them entirely. In fact, it was learned that the polishing activity, if done long enough (hours), would begin to create its own undulations of slightly different spatial frequency and amplitude.

Estimated slope error on the poor performing lens (original) was 5 $\mu\text{m}/\text{mm}$. Repolishing improved and lowered the amplitude of higher spatial-frequency undulations at various zones across the part, but as polishing time increased, asymmetry and polishing signature error grew. The “remade” asphere was ground with an extreme effort to reduce radial undulations by ultra fine grinding on an aerostatic and hydrostatic machine platform. During polishing, the polishing pad stiffened and the load was adjusted so undulation peaks were polished aggressively while the removal rates in the valleys were minimal. Resulting localized slope was estimated at 2 $\mu\text{m}/\text{mm}$.

A further qualitative interferometric check for asymmetries was instituted. Optimax asphere polishing at that time was not able to deterministically correct for rotationally asymmetry, such as the propeller shaped error illustrated in Fig. 14. Surfaces with this configuration required hand correction. This defect can be missed when relying on a single pass using a two-dimensional profilometer instruments like the Talysurf. The production aspheric lenses for the Gate Lens were ultimately scanned at three 30° increments to insure acceptable asymmetry error.

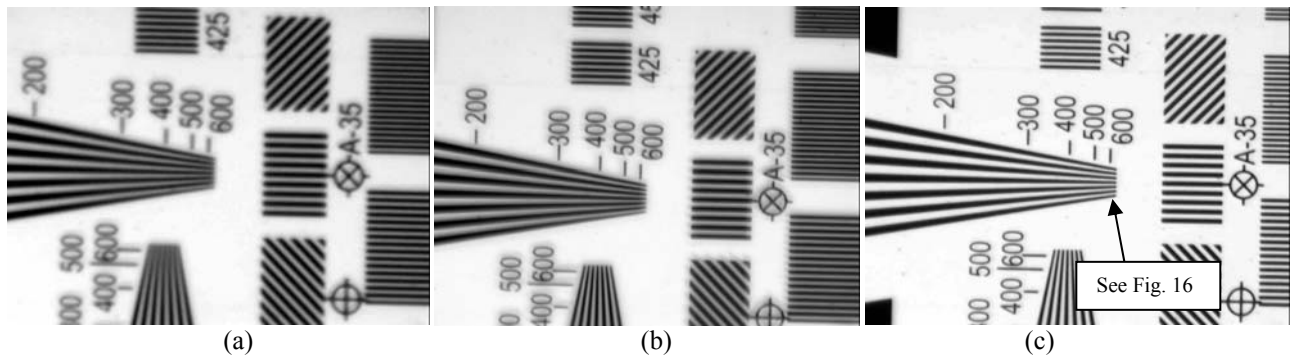


Figure 15. Image of resolution target. The original lens is (a), the repolished lens is (b), and the remade lens is (c). Note that the test system is operated in reverse of the actual telecine system, i.e., these are photographs of the target frame in the film gate imaged onto the CRT faceplate.

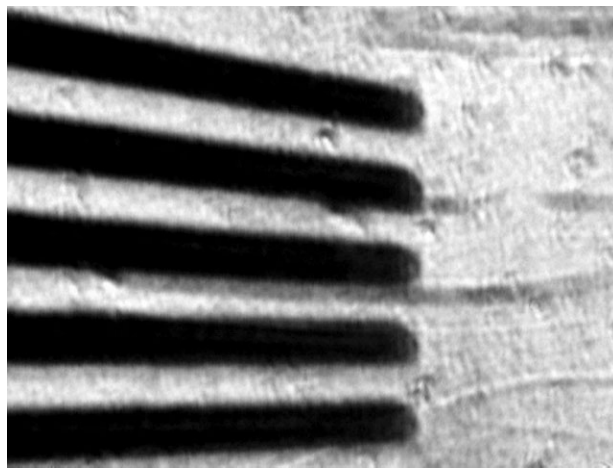


Figure 16. Close-up of resolution target is shown for remade lens at tip of the horizon fan pattern. See arrow in Fig. 10(c).

Images of the test resolution target are shown in Fig. 15 for the original aspheric lens, the repolished lens, and the remade lens. Examination of these images dramatically demonstrates the evolution of the aspheric surface and the achievement of the desired optical performance. Figure 16 shows a close-up of the tip of the horizontal resolution fan pattern shown in Fig. 15(c). The clarity and contrast are excellent. Based upon these results, production was started

with high yield, i.e., very few units made of this lens were found to have residual deficiencies at the system level testing that required rework.

5. CONCLUSIONS

Aspheric surfaces exhibit manufacturing artifacts that can be unique to the manufacturing process. The lens designer specifying surfaces in a manner that is clear to the fabricator and that can be verified by cost-effective metrology methods is critical to a successful outcome. At this time, the need for flexible 3-dimensional form testing for aspheres is paramount. Transmission test methods, with or without a null lens, only satisfy a small percentage of demands. Likewise, reflective surface tests using diffractive null lenses in concert with phase-measuring interferometers are often part-specific and can severely restrict $F/\#$. QED is making headway with their stitching interferometer product called the SSI and various other companies are working to develop alternative solutions using Shack-Hartmann Interferometry and automated three-dimensional profiling. All systems that are available or in development have entry prices of several hundred thousand dollars, so acceptance by the industry will be moderated by the high cost, but the need exists.

Rapid development of the aspheric glass lens was made possible by the interactive relationship between the optical designer, diamond-grinding personnel, and the metrology personnel. With rare exceptions, the subsequent production lenses achieved the required optical performance and afforded reasonable manufacturing costs.

REFERENCES

1. R. Barry Johnson, "Lenses," in Michael Bass (Ed. In Chief), *Handbook of Optics*, McGraw-Hill, New York, 1995, Vol. 2, p. 1.6.

APPENDIX

Program to Generate Grid Sag Data for ZEMAX

This program assumes that a single profilometer scan is made across the diameter of the part. The scan data are further assumed to be referenced to the even asphere parameters that the part was ideally to match. The program determines the sag at $[x=0, y=0]$ by using spline interpolation. The data are then offset such that the resultant grid sag data at $[x=0, y=0]$ is zero as required by ZEMAX.

Data read into the array "scan" is a two column array where the first column "X" contains the "x" coordinates and the second column "Y" contains the corresponding "sag" data. "Z" contains the spline interpolation data.

The program accounts for situations having an asymmetry by interpolating between + & - data with respect to the $[x=0, y=0]$ point for all $[x,y]$.

scan :=


 F:\A.11066M2.DAT

The input data format is two columns of numeric data. The first column contains the spatial scan data while the second column contains the residual sag data.

X := scan<0> Y := scan<1> Z := lspline(X, Y)

offset := interp(Z, X, Y, 0)

Y := Y - offset

Applies offset to measured sag data.

Z := lspline(X, Y)

Recomputes spline interpolation data.

User sets nx, ny, ϵ and maximum length of scan to be considered relative to $x=0$ (nominally half the length of total scan), rho_max.

nx := 255 ny := 255 ϵ := .25 rho_max := 30

A_{0,0} := nx A_{0,1} := ny A_{0,2} := ϵ A_{0,3} := ϵ

The "A" array is the output data for ZEMAX. The first line contains the header information.

Defines functions for computing sag and derivatives.

$$\text{sag}(x, y) := \begin{cases} \text{rho} \leftarrow \sqrt{x^2 + y^2} \\ \text{sag_plus} \leftarrow \text{interp}(Z, X, Y, \text{rho}) \\ \text{sag_minus} \leftarrow \text{interp}(Z, X, Y, -\text{rho}) \\ \text{d_sag} \leftarrow \text{sag_plus} - \text{sag_minus} \\ \text{sag_interp} \leftarrow \text{sag_minus} + \text{d_sag} \cdot \left[\frac{(x + \text{rho})}{2 \cdot \text{rho}} \right] & \text{if } \text{rho} > 0 \\ 0 & \text{otherwise} \end{cases}$$

$$d_sag_dx(x, y, \epsilon) := \begin{cases} sag_plus \leftarrow sag(x + \epsilon, y) \\ sag_minus \leftarrow sag(x - \epsilon, y) \\ s \leftarrow \frac{(sag_plus - sag_minus)}{2 \cdot \epsilon} \end{cases}$$

$$d_sag_dy(x, y, \epsilon) := \begin{cases} sag_plus \leftarrow sag(x, y + \epsilon) \\ sag_minus \leftarrow sag(x, y - \epsilon) \\ s \leftarrow \frac{(sag_plus - sag_minus)}{2 \cdot \epsilon} \text{ if } y \neq 0 \\ s \leftarrow \frac{(sag(x, \epsilon) - sag(x, 0))}{\epsilon} \text{ otherwise} \end{cases}$$

The final line considers the case of $d_sag/dy=0$ when $y=0$ (due to x-symmetry).

$$d2sag_dxdy(x, y, \epsilon) := \begin{cases} sag_plus \leftarrow sag(x + \epsilon, y + \epsilon) \\ sag_minus \leftarrow sag(x - \epsilon, y + \epsilon) \\ s1 \leftarrow \frac{(sag_plus - sag_minus)}{2 \cdot \epsilon} \text{ if } y \neq 0 \\ s1 \leftarrow \frac{(sag(x + \epsilon, \epsilon) - sag(x, \epsilon))}{\epsilon} \text{ otherwise} \\ sag_plus \leftarrow sag(x + \epsilon, y - \epsilon) \\ sag_minus \leftarrow sag(x - \epsilon, y - \epsilon) \\ s2 \leftarrow \frac{(sag_plus - sag_minus)}{2 \cdot \epsilon} \text{ if } y \neq 0 \\ s2 \leftarrow \frac{(sag(x + \epsilon, 0) - sag(x, 0))}{\epsilon} \text{ otherwise} \\ dx dy \leftarrow \frac{(s1 - s2)}{2 \cdot \epsilon} \text{ if } y \neq 0 \\ dx dy \leftarrow \frac{(s1 - s2)}{\epsilon} \text{ otherwise} \end{cases}$$

$j := 1 .. nx$

rows or "y"

$k := 1 .. ny$

columns or "x"

$$A_{((j-1) \cdot nx + k), 0} := \begin{cases} x \leftarrow \left[k - \frac{(nx + 1)}{2} \right] \cdot \epsilon \\ y \leftarrow - \left[j - \frac{(ny + 1)}{2} \right] \cdot \epsilon \\ rho \leftarrow \sqrt{x^2 + y^2} \\ s \leftarrow sag(x, y) \text{ if } rho < rho_max \\ 0 \text{ otherwise} \end{cases}$$

sag

$$A_{((j-1) \cdot nx+k),1} := \begin{cases} x \leftarrow \left[k - \frac{(nx+1)}{2} \right] \cdot \epsilon \\ y \leftarrow \left[j - \frac{(ny+1)}{2} \right] \cdot \epsilon \\ \rho \leftarrow \sqrt{x^2 + y^2} \\ s \leftarrow d_sag_dx(x, y, \epsilon) \text{ if } \rho < \rho_max \\ 0 \text{ otherwise} \end{cases} \quad d_sag/dx$$

$$A_{((j-1) \cdot nx+k),2} := \begin{cases} x \leftarrow \left[k - \frac{(nx+1)}{2} \right] \cdot \epsilon \\ y \leftarrow \left[j - \frac{(ny+1)}{2} \right] \cdot \epsilon \\ \rho \leftarrow \sqrt{x^2 + y^2} \\ s \leftarrow d_sag_dy(x, y, \epsilon) \text{ if } \rho < \rho_max \\ 0 \text{ otherwise} \end{cases} \quad d_sag/dy$$

$$A_{((j-1) \cdot nx+k),3} := \begin{cases} x \leftarrow \left[k - \frac{(nx+1)}{2} \right] \cdot \epsilon \\ y \leftarrow \left[j - \frac{(ny+1)}{2} \right] \cdot \epsilon \\ \rho \leftarrow \sqrt{x^2 + y^2} \\ s \leftarrow d2sag_dxdy(x, y, \epsilon) \text{ if } \rho < \rho_max \\ 0 \text{ otherwise} \end{cases} \quad d2_sag/dxdy$$

The element in A corresponding to the center (optical axis) of the grid sag array must be identically equal to zero in order for ZEMAX to work. The center element of A is computed by the following. Note the data array starts in line 1 while the header data are in line 0.

$$center := \frac{(nx \cdot ny + 2 \cdot nx + 3)}{2} \quad A_{center,0} := 0$$

WRITEPRN("gridsag.dat") := A